INT. J. NUMERICAL METHODS IN HEAT AND FLUID FLOW

Accepted September 14th 2016

ISSN: 0961-5539

PUBLISHER: EMERALD GROUP, UK

MAGNETO-NANOFLUID FLOW WITH HEAT TRANSFER PAST A STRETCHING SURFACE FOR THE NEW HEAT FLUX MODEL USING NUMERICAL APPROACH

Noreen Sher Akbar*
DBS&H CEME, National University of Sciences and Technology, Islamabad, **Pakistan.**
O. Anwar Bég
Fluid Mechanics, Biopropulsion and Nanosystems, Aeronautical and Mechanical Engineering, School of Computing, Science and Engineering, Newton Bldg, G77, University of Salford, Manchester, M54WT, **UK**
Zafar Hayat Khan
Department of Mathematics, University of Malakand, Dir (Lower), Khyber Pakhtunkhwa, **Pakistan**.
Dharmendra Tripathi
Department of Mechanical Engineering, Manipal University, Jaipur-303007, **India**

ABSTRACT

Sheet processing of magnetic nanomaterials is emerging as a new branch of smart materials manufacturing. The efficient production of such materials combines many physical phenomena including magnetohydrodynamics (MHD), nanoscale, thermal and mass diffusion effects. To improve understanding of complex inter-disciplinary transport phenomena in such systems, mathematical models provide a robust approach. Motivated by this, herein we develop a mathematical model for steady, laminar, magnetohydrodynamic, incompressible nanofluid flow, heat and mass transfer from a stretching sheet. A uniform constant strength magnetic field is applied transverse to the plane of the stretching flow. The Buonjiornio nanofluid model is employed to represent thermophoretic and Brownian motion effects. A non-Fourier (Cattaneo-Christov) model is deployed to simulate thermal conduction effects of which the Fourier model is a special case when thermal relaxation effects are neglected. The governing conservation equations are rendered dimensionless with suitable scaling transformations. The emerging nonlinear boundary value problem is solved with a fourth order Runge-Kutta algorithm and also shooting quadrature. Validation is achieved with earlier non-magnetic and forced convection flow studies. The influence of key thermophysical parameters e.g. Hartmann magnetic number, thermal Grashof number, thermal relaxation time parameter, Schmidt number, thermophoresis parameter, Prandtl number and Brownian motion number on velocity, skin friction, temperature, Nusselt number, Sherwood number and nano-particle concentration distributions is investigated. A strong elevation in temperature accompanies an increase in Brownian motion parameter whereas increasing magnetic parameter is found to reduce heat transfer rate at the wall (Nusselt number). Nano-particle volume fraction is observed to be strongly suppressed with greater thermal Grashof number, Schmidt number and thermophoresis parameter whereas it is elevated significantly with greater Brownian motion parameter. Higher temperatures are achieved with greater thermal relaxation time values i.e. the non-Fourier model predicts greater values for temperature than the classical Fourier model.

Corresponding Author

KEY WORDS: *Non-Fourier conduction; magnetic nanofluids; boundary layer flow; stretching sheet; Brownian motion; thermophoresis.*

NOMENCLATURE

C *nano-particle (solutal) concentration*	q *heat flux*
C_w *nano-particle (solute) concentration at the wall*	G_T *Thermal Grashof number*
C_∞ *ambient nano-particle concentration as y tends to infinity*	g *Acceleration due to gravity*
D_B *Brownian diffusion coefficient*	λ_2 *thermal relaxation time*
D_T *Thermophoretic diffusion coefficient*	B_C *Solutal Grashof number*
B_0 *magnitude of magnetic field strength*	v *Kinematic viscosity of the fluid*
T *Local fluid temperature*	P_r *Prandtl number*
T_∞ *Ambient temperature*	M *Hartmann Number*
u, v *Velocity components along x and y directions*	N_b *Brownian motion parameter*
P *pressure*	Sc *Schmidt number (= PrLe)*
ϕ *Nanoparticle volume fraction*	Re_x *Local Reynolds number*
η *Similarity variable (transformed coordinate)*	μ *Dynamic viscosity of nanofluid*
Nu_x *Local Nusselt number* Sh_x^n *Local nanoparticle Sherwood number*	Le *Regular Lewis number* x, y *Coordinate along and normal to the sheet*
$(\rho c)_p$ *Effective heat capacity of the nanoparticle material*	$(\rho c)_f$ *Heat capacity of the fluid*
θ *Dimensionless temperature*	*Nt Thermophoresis parameters*
γ *non-dimensional thermal relaxation time*	*K Thermal conductivity of the fluid*

1. INTRODUCTION

Nanoparticles provide a bridge between bulk materials and molecular structure. When deployed strategically in base fluids the resulting "nanofluids" have been proven to achieve exceptional enhancement in thermal conductivity properties, as identified by Choi [1]. This has made them

attractive in numerous areas of modern technology including aerospace cooling systems [2], heat exchangers [3] and energy systems [4]. When developing customized nanofluids for deployment in such applications, manufacturing processes exert a key influence on the constitution of final products. In materials processing a popular mechanism employed is that of *continuous sheet stretching*. The mathematical study of such flows was mobilized over five decades ago by Sakiadis who considered Newtonian flows from continuously moving surfaces [5]. This type of flow is particularly suitable to being simulated with *boundary layer theory*. Many subsequent studies have appeared examining heat and mass transfer in stretching boundary layer flows including Takhar *et al*. [6], Gorla *et al.* [7] and Hayat *et al*. [8]. More recently nanofluid stretching boundary layer flows have also been considered and representative works include Uddin *et a*l. [9], Rana and Bhargava [10], Nadeem *et al*. [11] and Rana *et al.* [12]. The two most popular approaches in simulating nanofluid boundary layer transport phenomena are either the *Buonjiornio model* (which invokes a separate species concentration boundary layer equation) and the *Tiwari-Das* model (which only requires momentum and energy boundary layer equations and simulates nano-particle effects via a volume fraction parameter). Many researchers have utilized these approaches including Nield and Kuznetsov [13], Rashidi *et al.* [14], Latiff *et al*. [15] and Ferdows *et al.* [16]. The vast majority of such studies have considered the classical Fourier model for thermal conduction heat transfer. However it has been identified that this model may not be accurate for certain situations as it produces a *parabolic energy equation* which implies that any initial thermal disturbance is instantly experienced by the medium under examination. A modification to the Fourier law is therefore necessitated and in this regard a robust model which has been proposed is the *Cattaneo-Christov non-Fourier model* [17-19]. This features a relaxation time for heat flux and results in a *hyperbolic energy equation* which successfully captures the flux of heat via propagation of thermal waves with finite speed. It is relevant to not only materials processing operations [20] but also bio-heat transfer [21]. A number of excellent studies have appeared recently employing the *Cattaneo-Christov non-Fourier model* including Mustafa [22] who studied rotating viscoelastic heat transfer and also Hayat *et al.* [23] who investigated melting in stretching sheet flow of a non-Newtonian fluid.

Magnetohydrodynamics (MHD) is the study of the interaction of magnetic fields (which may be static or oscillating) and electrically-conducting fluids. It is a subject of immense industrial importance in for example metallurgical processing and induction furnaces [24]. MHD also has significant emerging applications in biomagnetic flow control [25], Marangoni convection in biophysical suspensions [26], hemodynamics [27] and pharmaco-dynamics [28]. In this latter area it has also been exploited in targeted drug delivery where nano-particles are coated in magnetic

materials to assist in their directability in the human circulatory system. Furthermore in nuclear engineering systems, [29] magnetic nanofluids are also being examined, since they combine both the thermal enhancement properties of nanofluids with the magnetic manipulation properties of electrically-conducting liquids. The former can assist in for example cooling very high temperature surfaces and the latter permit manipulation of flow rates and also heat transfer characteristics [30]. It is therefore beneficial to investigate the thermofluid dynamics of magnetic nanofluid sheet processing as this provides further insight into the heat transfer, mass transfer and momentum characteristics of nanomaterials. The investigation of non-Fourier heat conduction phenomena also gives a more realistic appraisal of thermo-mechanics of nanofluids [31] which may be exploited strategically in reducing heat transfer rates of nuclear power technologies (both for civilian and future aerospace propulsion). Such analyses may also be of use in minimizing over-heating of hybrid deep-space rocket propulsion systems [32].

In the present study we therefore examine theoretically, for the first time, the steady, laminar, magnetohydrodynamic, incompressible nanofluid flow, heat and mass diffusion from a stretching sheet, as a model of magnetic nanomaterials fabrication. We adopt the Buonjiornio nanofluid model [33] which emphasizes thermophoretic and Brownian motion effects and introduces a separate nano-particle species diffusion equation. The Cattaneo-Christov non-Fourier thermal conduction model is also applied [34], which introduces a thermal relaxation effect. The normalized non-linear two-point boundary value problem is solved with numerical shooting quadrature. Validation with previous studies is included. The current study has to the authors' knowledge not appeared in the literature thusfar.

2. MATHEMATICAL FLOW MODEL

The regime under investigation is illustrated in **Fig. 1**. Two-dimensional, steady-state, incompressible flow of an electrically-conducting nanofluid from a vertical stretching sheet is considered, with reference to an (*x*,*y*) coordinate system, where the x-axis is aligned with the sheet. A transverse static uniform strength magnetic field is applied, which is sufficiently weak to negate magnetic induction and Hall current effects. The nanofluid is dilute and comprises a homogenous suspension of equally-sized nanoparticles in thermal equilibrium [35]. The sheet is stretched in the plane $y = 0$. The flow is assumed to be confined to $y > 0$. Here we assumed that the sheet is uniformly extended with the linear velocity $u(x) = ax$, where $a > 0$ is constant and *x*-axis is measured along the stretching surface. Under these assumptions, the governing conservation equations for mass, momentum, energy (heat) and

nano-particle species diffusion, neglecting viscous and Joule dissipation effects, may be shown to take the form:

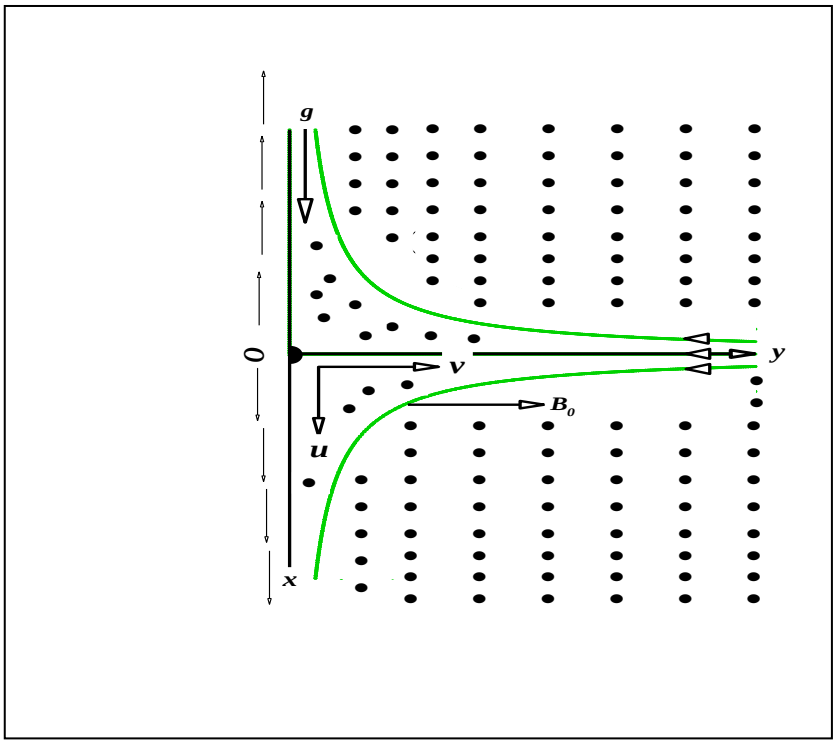

Fig.1. Physical model for the magnetohydrodynamic nanofluid stretching sheet problem.

$$\frac{\partial u}{\partial x}+\frac{\partial v}{\partial y}=0, \tag{1}$$

$$\left(u\frac{\partial u}{\partial x}+v\frac{\partial u}{\partial y}\right)=\nu\left(\frac{\partial^2 u}{\partial y^2}\right)-\frac{\sigma B_o^2}{\rho}u+\rho g\beta_T\left(T-T_\infty\right)+\rho g\beta_C\left(C-C_\infty\right), \tag{2}$$

$$\rho\left(c_p\right)\bar{v}.\nabla T=-\nabla.q+\tau\left[D_B\frac{\partial T}{\partial y}\frac{\partial C}{\partial y}+\left(\frac{D_T}{T_\infty}\right)\left(\frac{\partial T}{\partial y}\right)^2\right], \tag{3}$$

$$\left(u\frac{\partial \phi}{\partial x}+v\frac{\partial \phi}{\partial y}\right)=D_B\frac{\partial^2 C}{\partial y^2}+\left(\frac{D_T}{T_\infty}\right)\frac{\partial^2 T}{\partial y^2}. \tag{4}$$

Here $\tau=\dfrac{(\rho c)_p}{(\rho c)_f}$ is the ratio of the effective heat capacity of the nano-particles to the base fluid, u and v are the velocity components along the x and y-directions respectively, T is the temperature of the magnetic nanofluid, B_0 is the magnitude of magnetic field strength, q is the heat flux. In Eq. (3) we employ the Cattaneo–Christov thermal conduction model for heat flux, which has the following form:

$$q+\lambda_2\left(\frac{\partial q}{\partial t}+V.\nabla.q-q.\nabla V+(\nabla.V)q\right)=-K\ \nabla T, \tag{5}$$

Here λ_2 is the *thermal relaxation time*. Eliminating q from Eqns. (3) and (5), the modified energy conservation equation then assumes the form:

$$\begin{aligned}&\left(u\frac{\partial T}{\partial x}+v\frac{\partial T}{\partial y}\right)+\lambda_2\left(u\frac{\partial u}{\partial x}\frac{\partial T}{\partial x}+v\frac{\partial v}{\partial y}\frac{\partial T}{\partial y}+u\frac{\partial v}{\partial x}\frac{\partial T}{\partial y}+v\frac{\partial u}{\partial y}\frac{\partial T}{\partial x}+2uv\frac{\partial^2 T}{\partial x\partial y}+u^2\frac{\partial^2 T}{\partial x^2}+v^2\frac{\partial^2 T}{\partial y^2}\right)\\&=\frac{K}{\rho(c_p)}\frac{\partial^2 T}{\partial y^2}+\tau\left[D_B\frac{\partial T}{\partial y}\frac{\partial C}{\partial y}+\left(\frac{D_T}{T_\infty}\right)\left(\frac{\partial T}{\partial y}\right)^2\right],\end{aligned} \tag{6}$$

Here T is the nanofluid temperature, P is the pressure and the other physical quantities are defined in the nomenclature. We note that when $\lambda_2 \to 0$, the thermal relaxation effect is negated and the Cattaneo–Christov thermal conduction model reduces to the *classical Fourier conduction law*. Essentially therefore the presence of thermal relaxation makes the energy conservation equation a *non-Fourier* model. The boundary conditions are prescribed as follows:

$$u=u_w(x)=ax,\quad v=0,\quad T=T_w,\quad C=C_w,\ \text{at y = 0.} \tag{8}$$

$$u\to 0,\quad v\to 0,\quad T\to T_\infty,\quad C\to C_\infty,\ \text{as}\ y\to\infty. \tag{9}$$

To facilitate numerical solutions to the primitive boundary value problem, it is pertinent to introduce the following similarity transformations and dimensionless variables:

$$u=axf'(\eta),\ v=-\sqrt{(a\nu)}f(\eta),\quad \eta=\sqrt{\left(\frac{a}{\nu}\right)}y,\quad \theta(\eta)=\frac{T-T_\infty}{T_w-T_\infty},\ \phi(\eta)=\frac{C-C_\infty}{C_w-C_\infty}, \tag{10}$$

Implementing eqn. (9) in the conservation eqns. (1), (2), (4) and (6), the following nonlinear, coupled system of self-similar ordinary differential equations emerges:

$$f'''-(f')^2+ff''-M^2f'+G_r\theta+B_r\Phi=0, \tag{11}$$

$$\frac{1}{\Pr}\theta''+f\theta'+N_b\theta'\xi'+N_t(\theta')^2-\gamma\left(ff'\theta'+f^2\theta''\right)=0, \tag{12}$$

$$\phi''+Scf\phi'+\frac{N_t}{N_b}\theta''=0, \tag{13}$$

The transformed boundary conditions assume the form:

$$f(0)=0,\quad f'(0)=1,\ \theta(0)=1,\ \phi(0)=1, \tag{13a}$$

$$f'(\infty)=0,\quad \theta(\infty)=0,\ \phi(\infty)=0, \tag{13b}$$

where primes denote differentiation with respect to η i.e. the transformed transverse coordinate. Furthermore the following dimensionless numbers are invoked in eqns. (10)-(12):

$$M^2=\frac{\sigma B_0^{\,2}}{\rho\, a},\quad R_{ex}=\frac{u_w(x)x}{\nu},\ G_T=\frac{\rho g x^3\beta_T(T_w-T_\infty)}{\nu^2},\ G_r=\frac{G_T}{R_{ex}^{\,2}},$$

$$\Pr=\frac{\nu}{\alpha},\ N_b=\frac{\tau D_B(\phi_w-\phi_\infty)}{\nu},\ N_t=\frac{\tau D_T(T_w-T_\infty)}{\nu T_\infty},\quad Sc = PrLe,\ \gamma=a\lambda_2, \tag{14}$$

$$B_T=\frac{\rho g x^3\beta_C(C_w-C_\infty)}{\nu^2},\ B_r=\frac{B_T}{R_{ex}^{\,2}}.$$

These represent respectively the square of the *Hartmann magnetic body force number, local Reynolds number, thermal Grashof number* (ratio of *thermal buoyancy force* to *viscous force, thermal buoyancy ratio parameter, Prandtl number, Brownian motion parameter, thermophoresis parameter, Schmidt number, thermal relaxation parameter, solutal (species) Grashof number* (ratio of *concentration buoyancy force* to *viscous force*), and *species buoyancy ratio parameter*. Expressions for the skin friction coefficient (wall shear stress function), local Nusselt number (wall heat transfer rate) and the local Sherwood number (wall nano-particle mass transfer rate) may also be defined as follows:

$$C_f=\frac{\tau_w}{\rho u_w^{\,2}}, Nu=\frac{xq_w}{\alpha(T_w-T_\infty)},\quad Sh=\frac{xq_m}{\alpha(C_w-C_\infty)}, \tag{15}$$

$$\tau_w=\mu\left(\frac{\partial u}{\partial y}\right),\quad q_w=-\alpha\left(\frac{\partial T}{\partial y}\right),\qquad q_m=-\alpha\left(\frac{\partial C}{\partial y}\right), \tag{16}$$

$$\mathrm{Re}_x^{1/2}C_f=f''(0),\ \mathrm{Re}_x^{-1/2}Nu_x=-\theta'(0),\ \mathrm{Re}_x^{-\frac{1}{2}}Sh_x=-\phi'(0), \tag{17}$$

It is important to note that the present boundary value problem reduces to the classical problem of magnetohydrodynamic flow, and heat and mass transfer due to a stretching surface in a viscous fluid when *Nb* and *Nt* $\rightarrow 0$ neglecting nanoscale effects, in Eqns. (10) and (11). Furthermore the non-Fourier model contracts to the classical Fourier model when $\gamma\rightarrow 0$ i.e. thermal relaxation time effects vanish. The functions defined in eqns. (15)-(17) provide an important estimate of the wall heat and mass transfer characteristics which are useful in materials processing design.

3. NUMERICAL SOLUTIONS OF TRANSFORMED EQUATIONS AND VALIDATION

The nonlinear ordinary differential equations (10)-(12) subject to the boundary conditions (13) have been solve numerically using an efficient Runge–Kutta fourth order method along with a shooting technique. The asymptotic boundary conditions given by Eq. (13) were replaced by using a value of 15 for the similarity variable $\eta_{\max}$. The choice of $\eta_{\max} = 15$ and the step size $\Delta\eta = 0.001$, ensured that all numerical solutions approached the asymptotic values correctly. For validation of the proposed scheme, a comparison for the Nusselt number with the literature [36, 37] has been shown in **Table 1,** for the magnetohydrodynamic case without thermal buoyancy. Furthermore additional benchmarking of solutions has been documented in **Table 2** with non-magnetic, Fourier-model based solutions given earlier in [38-41]. Very good correlation is achieved for all values of Hartmann number (*M*) in **Table 1** and for all Prandtl numbers (*Pr*) in **Table 2** with published solutions.

Table 1 Comparison of results for skin friction for ($G_r = 0$).

M	Present results	Salahuddin *et al.* [36]	Akbar *et al.* [37]
0.0	1	1	1
0.5	-1.11803	-1.11801	-1.11803
1	-1.41421	-1.41418	-1.41421
5	-2.44949	-2.44942	-2.44949
10	-3.31663	-3.31656	-3.31663
100	-10.04988	-10.04981	-10.04988
500	-22.38303	-22.38393	-22.38303
1000	-31.63859	-31.63846	-31.63859

Table 2 Comparison of results for Nusselt number for pure fluid i.e, $Nt = Nb = 0$ with $M = 0$, $\gamma = 0$ and $G_r = 0$.

Pr	Present results	Khan *et al.* [38]	Khan & Pop [39]	Wang [40]	Kandasamy *et al.* [41]
0.07	0.0663	0.0663	0.0663	0.0656	0.0661
0.20	0.1691	0.1691	0.1691	0.1691	0.1691
0.70	0.4539	0.4539	0.4539	0.4539	0.4542
2	0.9114	0.9114	0.9113	0.9114	0.9114
7	1.8954	1.8954	1.8954	1.8954	1.8952

20	3.3539	3.3539	3.3539	3.3539	--
70	6.4622	6.4622	6.4621	6.4622	--

In these Tables, skin friction is shown to decrease significantly with greater *M* value whereas Nusselt number is observed to be consistently elevated with greater *Pr* value (which is a thermophysical property of a particular fluid). The former is attributable to the decelerating effect of magnetic field via the Lorentzian magnetohydrodynamic drag. The latter is caused by the decrease in thermal conductivity of fluids with greater Prandtl number which enhances heat transfer to the wall, reduces temperatures in the body of the fluid and thereby elevates Nusselt number. Therefore, we are confident that the applied numerical scheme is very accurate.

4. RESULTS AND DISCUSSION

Extensive numerical computations have been conducted. The results are depicted in **Figs.2–7** in which the influence of selected parameters on momentum, heat, and mass transfer characteristics are presented graphically.

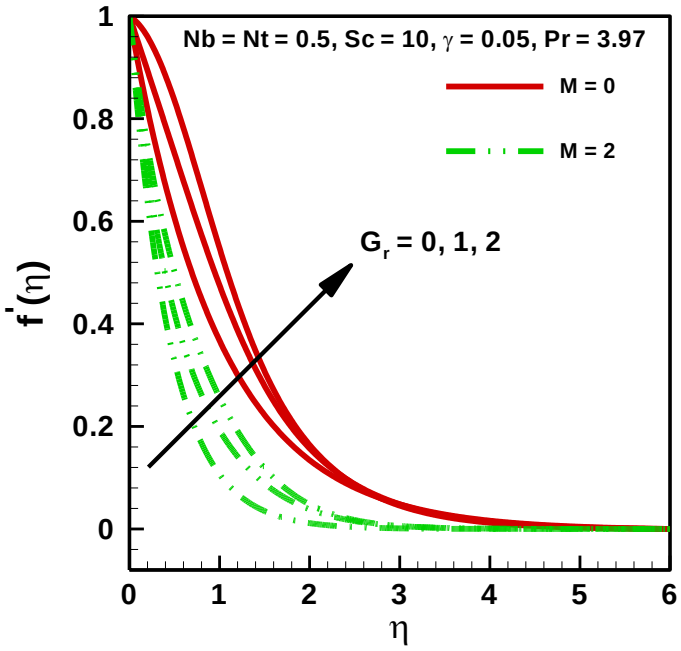

Fig. 2. Velocity profile for different values of thermal buoyancy ratio (G_r) and Hartmann number (M).

Evidently a significant acceleration accompanies an increase in thermal buoyancy ratio (G_r), since thermal buoyancy (free convection current) effect aids in momentum diffusion in the boundary layer. Gr in fact defines the ratio of thermal Grashof number to the square of Reynolds number and

invokes therefore not just thermal buoyancy force and viscous force but also inertial force. This has been emphasized in many seminal works in buoyancy-driven flows, notably by Gebhart *et al*. [42]. It has also been observed in other studies of nanofluid dynamics, for example Gorla *et al*. [43] and Nadeem *et al*. [44]. Thermal buoyancy encourages flow but reduces the momentum boundary layer thickness. It is therefore a primary mechanism used in materials processing operations to generate greater momentum flux. Conversely increasing Hartmann number, which symbolizes the relative contribution of *Lorentzian magnetohydrodynamic drag force* to *viscous hydrodynamic force*, results in a strong deceleration in nanofluid boundary layer flow. The velocity is therefore markedly decreased with greater *M* value and the momentum boundary layer thickness is increased. This has also been observed in other studies of magnetic nanofluid boundary layers, including [45].

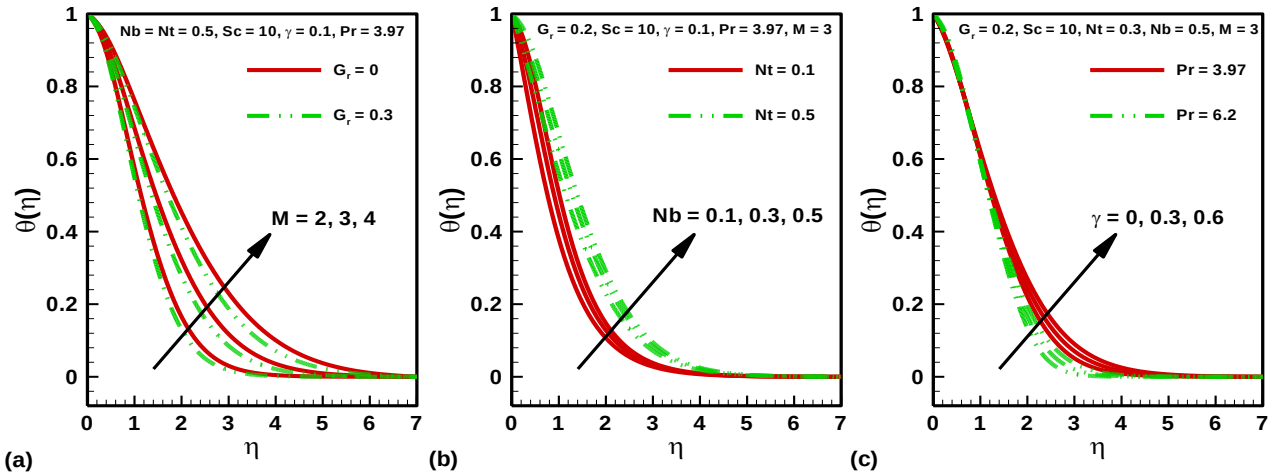

Fig. 3. Temperature profiles for different values of (a). Hartmann number (*M*) and thermal buoyancy ratio (G_r) (b). Brownian motion parameter (N_b) and thermophoresis parameter (N_t). (c) thermal relaxation time (γ) and Prandtl number (*Pr*).

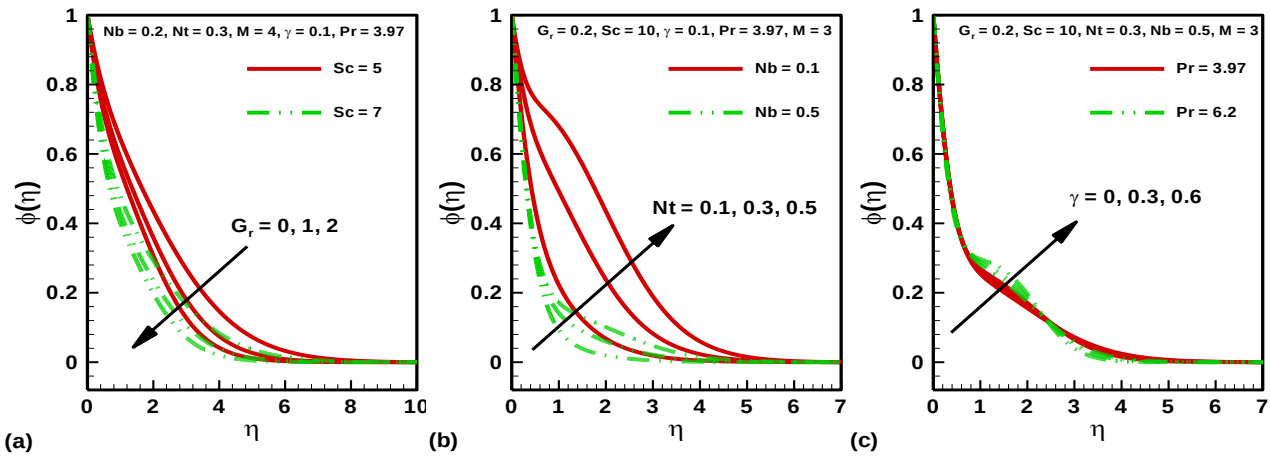

Fig. 4. Nanoparticle volume fraction (species concentration) profiles for different values of (a). thermal buoyancy ratio (G_r) and Schmidt number (*Sc*). (b). Brownian motion parameter (N_b) and thermophoresis parameter (N_t) (c) thermal relaxation time (γ) and Prandtl number (*Pr*).

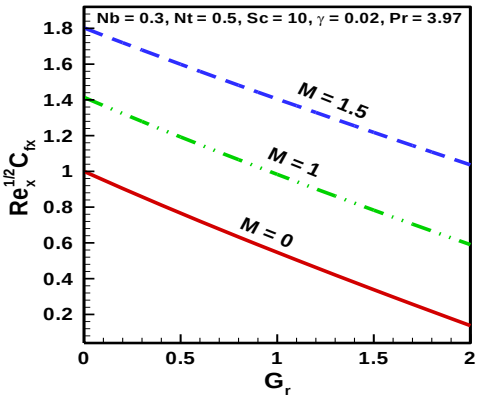

Fig. 5. Skin friction coefficient for different values of Hartmann number (M) and thermal buoyancy ratio (G_r).

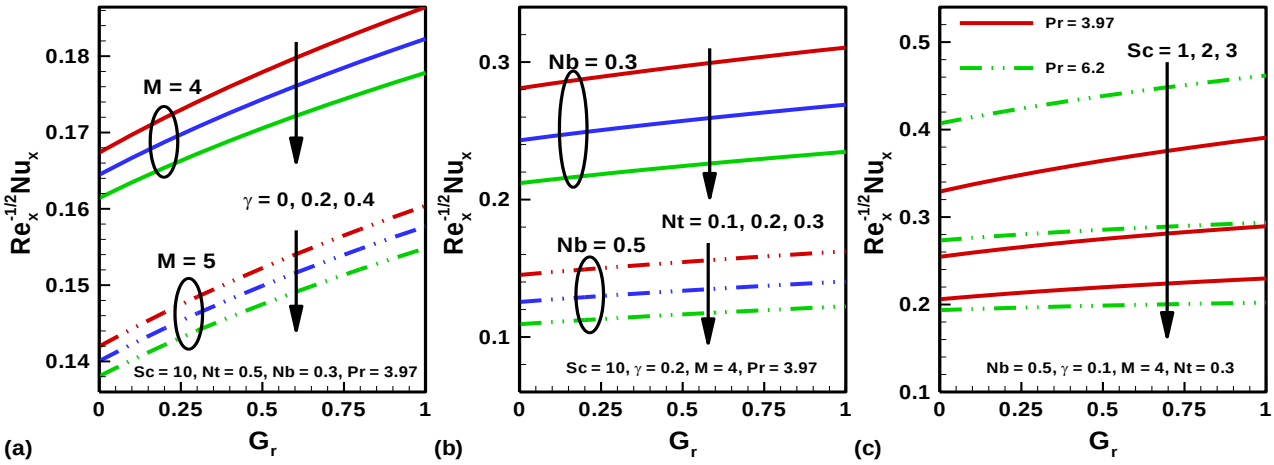

Figs. 6. Nusselt number for different values of (a) non-dimensional thermal relaxation time (γ), Hartmann number (M) and thermal buoyancy ratio (G_r).(b) Brownian motion parameter (Nb), Thermophoresis parameter (Nt) and thermal buoyancy ratio (G_r). (c). Schmidt number (Sc), Prandtl number (Pr) and thermal buoyancy ratio (G_r).

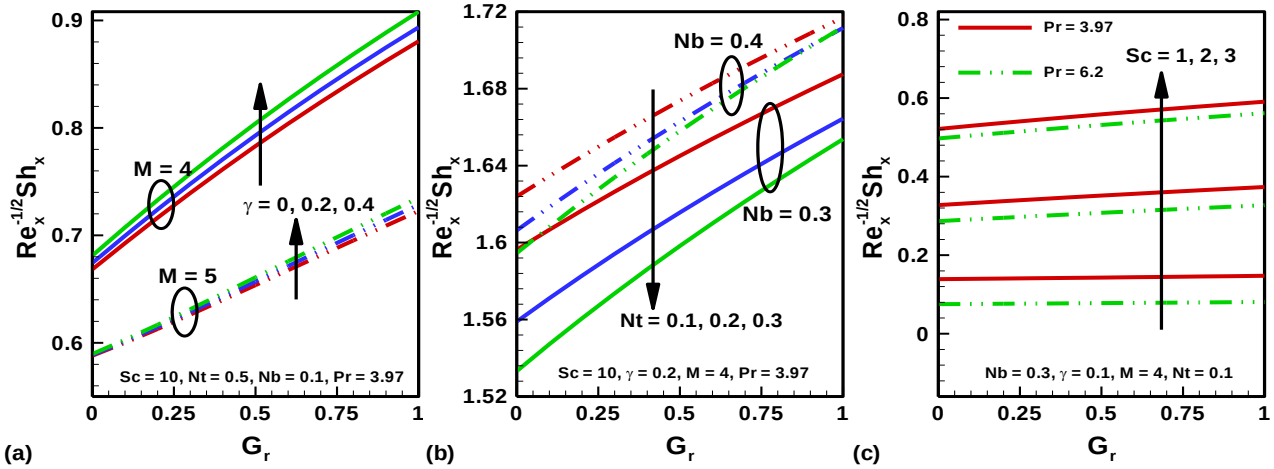

Fig. 7. Local Sherwood number for different values of (a) non-dimensional thermal relaxation time (γ), Hartmann number (M) and thermal buoyancy ratio (G_r).(b) Brownian motion parameter (Nb), Thermophoresis parameter (Nt) and thermal buoyancy ratio (G_r). (c). Schmidt number (Sc), Prandtl number (Pr) and thermal buoyancy ratio (G_r).

The asymptotically smooth profiles computed in fig. 2 also testify to the selection of an adequately large infinity boundary condition. Velocity profiles descend sharply from the sheet surface indicating that there is a deceleration in the nanofluid flow for relatively short migration into the thickness of the boundary layer. The weak nature of the magnetic field (M=2 is the maximum Hartmann number studied and corresponds to the Lorentzian force being double the viscous force) manifests in a distinct absence of any velocity overshoot at or near the wall. A similar response has been reported by Uddin *et al*. [46] also for magnetized nanofluids.

Figs 3a-c illustrate the collective effects of several key parameters on temperature distribution, $\theta(\eta)$. Evidently in fig. 3a a marked enhancement in temperature accompanies a rise in Hartmann number. The supplementary work expended in dragging the nanofluid against the imposed transverse magnetic field is dissipated as thermal energy. This results in a heating of the nanofluid regime and increase in thermal boundary layer thickness. Indeed this effect has been computed by numerous researchers for both viscous conducting and nanofluids- see for example Sutton and Sherman [47] and Mustafa *et al*. [48]. With increasing thermal buoyancy ratio however there is a slight depletion in temperatures. Thermal buoyancy force is known to cool boundary layer flows while simultaneously accelerating them, as emphasized by Gebhart *et al*. [42]. In fig. 3b we observe that an increase in Brownian motion parameter (Nb) strongly elevates temperatures. Larger magnitudes of Nb physically corresponds to smaller particles and vice versa for smaller values of Nb. Smaller particles are able to enhance thermal conduction in the nanoscale and this globally results in increase in the bulk temperature of the fluid, as highlighted by Choi [1] and later by Buonjiornio [33]. Although other mechanisms may contribute to thermal conductivity enhancement such as ballistic collisions and macro-convection, one of the dominant mechanisms (certainly for laminar flows) is now believed to be Brownian motion. The influence of the other key mechanisms, namely thermophoresis, is also depicted in fig. 3b. Greater values of thermophoresis parameter (Nt) are also observed to elevate temperatures and therefore increase thermal boundary layer thickness. Thermophoresis encourages nanoparticle transport away from a hotter surface towards a colder zone. This results in transport of thermal energy into the body of nanofluid and thereby increases temperatures. With increasing Prandtl number (Pr), there is a significant reduction in temperature, as shown in fig. 3b. We consider $Pr > 1$ implying that momentum diffusivity greatly exceeds the thermal diffusivity in the fluid. For greater Pr values, thermal conductivity in the fluid must also decrease and this explains the decrease in temperature as Pr ascends from 3.97 to 6.2. Thermal boundary layer thickness will therefore also be reduced in the nanofluid sheet regime. With increasing thermal relaxation parameter (γ) the nanofluid temperature is noticeably elevated.

Therefore the Fourier model (γ) evidently under-predicts nanofluid temperatures, whereas the non-Fourier model ($\gamma > 0$) produces greater magnitudes of temperature. The implications for materials processing is that a better estimate of actual temperatures can be achieved with the non-Fourier (*Cattaneo-Christov*) model via a relative simple modification of the heat conduction model. This may have an impact on better designing nanomaterials for specific applications.

Figs 4a-c illustrate the combined effects of a number of thermophysical parameters on the nano-particle volume fraction (species concentration), $\phi(\eta)$, in the boundary layer. An increase in Schmidt number (*Sc*) as displayed in fig. 4a clearly enhances the nano-particle volume fraction i.e. encourages nano-particle diffusion in the boundary layer. Nano-particle species (concentration) boundary layer thickness will therefore also be increased. The Schmidt number embodies the ratio of momentum diffusivity to species (nano-particle) diffusivity. When $Sc > 1$, as studied in this paper, momentum diffusion rate exceeds species diffusion rate. As Sc increases from 6 to 7, this results in slower nano-particle migration which manifests in a depleted concentrations of nano-particles although a more homogenous distribution throughout the boundary layer transverse to the sheet plane is achieved. Schmidt number is therefore a key parameter via which nano-particle transport can be manipulated. Increasing thermal buoyancy ratio (G_r) generates a similar effect and also reduces nano-particle volume fraction. Therefore greater thermal buoyancy force simultaneously decreases nano-particle concentration boundary layer thickness. In fig. 4b we observe that while increasing thermophoresis parameter (*Nt*) substantially boosts the nano-particle concentration, an increase in Brownian motion parameter (*Nb*) has the contrary influence and considerably suppresses nano-particle volume fraction magnitudes. With increasing Prandtl number (*Pr*) as shown in fig. 4c, the nano-particle volume fraction is initially elevated in close proximity to the wall but thereafter the effect is reversed as we approach the free stream. Further from the wall the nano-particle (volume fraction) magnitudes are slightly decreased. With greater thermal relaxation effect, in fig. 4c, there is a weak elevation in nano-particle concentration values. This is understandable since the effect is achieved indirectly via the coupling of the energy and species diffusion boundary layer equations. The prominent influence of thermal relaxation is on temperatures and a diminished effect is sustained therefore by the nano-particle concentration field.

Fig. 5 presents the evolution in skin friction (dimensionless surface shear stress) i.e. velocity gradient wat the wall, with Hartmann number (*M*) and thermal buoyancy ratio (G_r). There is a strong elevation in skin friction with greater magnetic field strength to which the Hartmann number is proportional. The profiles are all linear and maximized at low values of thermal buoyancy ratio and minimized at high values of thermal buoyancy ratio. Clearly therefore increasing thermal

buoyancy effect decelerates the boundary layer flow (decreases skin friction) and also serves to elevate momentum boundary layer thickness.

Figs 6a-c show the response in wall heat transfer rate i.e. Nusselt number with various thermo-physical parameters. In fig 6a an increase in Hartmann number (M) clearly suppresses Nusselt number implying a decrease in heat transported to the wall. This agrees with our earlier computations of temperature response (fig. 3a) since higher magnetic field body force will heat the nanofluid boundary layer and this will transfer heat into the body of the fluid away from the wall. Higher thermal relaxation (γ) values again also induce a fall in Nusselt number values and this is explained by the increase in temperatures (fig. 3c) described earlier. This causes the decrease in Nusselt number at the wall. Higher thermal buoyancy ratio (G_r) however elevates the Nusselt number and physically this is consistent with the depletion in temperatures computed in fig. 3a with greater thermal buoyancy force effect. With increasing thermophoresis parameter (Nt), as plotted in fig. 6b, Nusselt number is also depressed and again this is due to the elevation in temperatures within the nanofluid boundary layer regime with greater thermophoretic effect (as computed earlier in fig. 3b).With stronger Brownian motion (higher Nb values), again Nusselt number is reduced and once again this is directly attributable to the elevation in temperatures within the nanofluid sheet (fig. 3b). Heat transfer rate to the wall must therefore simultaneously decreases. Fig 6c shows that the Nusselt number is enhanced with greater Prandtl number (Pr) but suppressed with greater Schmidt number. Increasing thermal buoyancy force (higher G_r values) however generate a steady ascent in Nusselt number magnitudes implying that greater heat is transferred to the sheet (wall) with larger thermal buoyancy force since the boundary layer is cooled and thermal boundary layer thickness is decreased.

Figs 7a-c present the evolution of local Sherwood number (dimensionless nano-particle wall mass transfer rate) with various thermal, magnetic and nanoscale parameters. Increasing Hartmann magnetic parameter (M) is found to considerably reduce Sherwood number i.e. greater magnetic field applied transverse to the sheet results in a decreased migration of nano-particles towards the wall, since nano-particle concentrations in the boundary layer are elevated (as shown earlier). Conversely greater thermal relaxation time (γ) very strongly enhances local Sherwood number magnitudes, for any magnetic field scenario. Evidently greater thermal relaxation therefore encourages mass diffusion of nano-particles towards the wall (sheet). With greater thermal buoyancy effect (higher G_r values) local Sherwood number is also markedly and steadily elevated as testified to by the linear nature of the ascending profiles. Fig 7b shows that with increasing Brownian motion parameter (Nb), there is a strong elevation in local Sherwood number values,

irrespective of the values of thermophoresis parameter (Nt) and thermal buoyancy ratio (G_r). This increase is due to the elevated migration of nano-particles towards the wall with greater Brownian motion (smaller particle size) effect. On the other hand, an increase in thermophoresis parameter (Nt) generates the opposite effect and significantly depresses local Sherwood number since it elevates nano-particle concentrations within the nanofluid body regime. An increase in G_r values (greater thermal buoyancy effect) consistently enhances mass transfer rates to the wall and results in an increase in local Sherwood number magnitudes. Fig. 7c shows that while increasing Schmidt number elevates the local Sherwood number values very considerably, a rise in Prandtl number has the converse effect (although weaker) and noticeably reduces local Sherwood number. Increasing thermal buoyancy ratio (G_r) once again achieves a steady elevation in local Sherwood number magnitudes, although the rate of ascent is much less pronounced than in figs 7a and b.

5. CONCLUSIONS

A mathematical model has been developed to simulate the steady, laminar, magnetohydrodynamic, incompressible electrically-conducting nanofluid flow, heat and mass transfer from a stretching sheet in the presence of a transverse static magnetic field. The Buonjiornio nanofluid formulation has been adopted which invokes a species diffusion equation for the nano-particle migration. The non-Fourier Cattaneo-Christov heat flux model has also been employed to provide a more realistic estimation of temperature distribution in actual nanofluids. Via suitable scaling transformations and the deployment of carefully selected dimensionless variables, the dimensionless nonlinear partial differential conservation equations have been transformed to an ordinary differential boundary value problem with appropriate boundary conditions. A numerical solution has been presented based on an optimized fourth order Runge-Kutta algorithm combined with shooting quadrature. The solutions have been validated, where possible, with earlier published results for non-magnetic and forced convection (buoyancy absent) scenarios. The emerging boundary value problem has been shown to be dictated by a number of key thermophysical parameters, namely Hartmann (magnetic body force) number, thermal buoyancy ratio, thermal relaxation time parameter, Schmidt number, thermophoresis parameter, Prandtl number and Brownian motion number. The influence of these parameters has been computed for velocity, skin friction, temperature, Nusselt number, Sherwood number and nano-particle concentration distributions. The present investigation has shown that:

(i)Increasing Brownian motion parameter strongly elevates temperatures and local Sherwood number values whereas it decreases nano-particle volume fraction and Nusselt number values.

(ii) Increasing magnetic parameter is found to decelerate the boundary layer flow (i.e. reduce velocities) and also reduce heat transfer rate at the wall (Nusselt number) whereas it enhances temperatures and local Sherwood number magnitudes.
(iii) Increasing thermal buoyancy parameter significantly decreases nano-particle volume fraction whereas it weakly reduces temperatures in the nanofluid.
(iv) Increasing thermal relaxation time (i.e. the non-Fourier model) markedly elevates temperatures throughout the boundary layer whereas initially it weakly increases nano-particle volume fraction (species concentration) and thereafter slightly depresses magnitudes towards the boundary layer free stream. The Fourier heat conduction model (vanishing thermal relaxation time) under-predicts temperatures compared with the non- Fourier model.
(v) Increasing thermophoresis parameter increases both temperatures and nano-particle volume fraction, whereas it decreases both the Nusselt number and local Sherwood number.
(vi) Increasing Schmidt number reduces the Nusselt number whereas it elevates the local Sherwood number.
(vii) Increasing Prandtl number strongly elevates Nusselt number whereas it weakly reduces the local Sherwood number.

The present study has been confined to Newtonian nanofluids. Future investigations will consider rheological aspects and will be communicated imminently.

REFERENCES

[1] Choi. S. Enhancing thermal conductivity of fluids with nanoparticle. In: *Developments and applications of non-Newtonian flow, ASME Fluids Engineering Division*-vol.231/MD-vol.66; 99–105(1995).

[2] Narvaez, J.A., Aaron R. Veydt and Robert J. Wilkens, Evaluation of nanofluids as potential novel coolant for aircraft applications: the case of de-ionized water-based alumina nanofluids, *ASME J. Heat Transfer* 136(5), 051702 (2014).

[3] G. Huminic and A. Huminic, Application of nanofluids in heat exchangers: A review, *Renewable and Sustainable Energy Reviews*, 16, 5625–5638 (2012)

[4] Bég, O.A., R.S.R. Gorla, V. R. Prasad, B.Vasu and Rana D. Prashad, Computational study of mixed thermal convection nanofluid flow in a porous medium, *12th UK National Heat Transfer Conference, 30th August-1st September, Chemical Engineering Department, University of Leeds, UK* (2011).

[5] Sakiadis, B.C., Boundary layer behavior on continuous solid surfaces. ii: the boundary layer on a continuous flat surface, *AIChE Journal*, 7, 221-225 (1961).

[6] Takhar, H.S., Agarwal, R.S., Bhargava, R. and Jain, S., Mixed convection flow of a micropolar fluid over a stretching sheet, *Heat and Mass Transfer*, 34 (2-3), 213-219 (1998).

[7] Gorla, R.S.R. and I. Sidawi, Free convection on a vertical stretching surface with suction and blowing. *Appl. Sci. Res.*, 52, 247–257 (1994).

[8] Hayat T, Awais M, Sajid M., Mass transfer effects on the unsteady flow of UCM fluid over a stretching sheet. *Int. J. Mod. Phys. B*, 25: 2863–2878 (2011).

[9] Uddin, M.J., O. Anwar Bég and A.I. Ismail, Radiative-convective nanofluid flow past a stretching/shrinking sheet with slip effects, *AIAA J. Thermophysics Heat Transfer*, 29, 3, 513-523 (2015).

[10] Rana, P. and Bhargava, R. Flow and heat transfer over a nonlinearly stretching sheet: A numerical study. *Comm. Nonl. Sci. and Numer. Simulat.* 17, 212-226(2012).

[11] Nadeem S, Mehmood R, Akbar N S., Non-orthogonal stagnation point flow of a nano non-Newtonian fluid towards a stretching surface with heat transfer, *Int. J. Heat Mass Transfer*, 57: 679–689 (2013).

[12] Rana, P., Bhargava, R. and Anwar Bég, O. Finite element simulation of unsteady magneto-hydrodynamic transport phenomena on a stretching sheet in a rotating nanofluid, *Proc IMechE-Part N-J. of Nanoeng. and Nanosys.*, 227, 77-99 (2013).

[13] Nield, D.A. and Kuznetsov, A.V., The Cheng–Minkowycz problem for natural convective boundary-layer flow in a porous medium saturated by a nanofluid, *Int. J. Heat Mass Transfer*, 52, 5792–5795 (2009).

[14] Rashidi, M.M., N. Freidoonimehr, A. Hosseini,·O. Anwar Bég, T.-K. Hung, Homotopy simulation of nanofluid dynamics from a non-linearly stretching isothermal permeable sheet with transpiration, *Meccanica*, 49, 469-482 (2014).

[15] Latiff, N.A., M.J.. Uddin, O. Anwar Bég and Ahmad Izani Md. Ismail, Unsteady forced bioconvection slip flow of a micropolar nanofluid from a stretching/ shrinking sheet, *Proc. IMechE-Part N: J. Nanoengineering and Nanosystems (2015). DOI: 10.1177/1740349915613817*

[16] Ferdows, M., Md. S. Khan and O. Anwar Bég, Numerical study of transient magnetohydrodynamic radiative free convection nanofluid flow from a stretching permeable surface, *Proc IMechE-Part E: J. Process Mechanical Engineering*, 228, 181-196 (2014).

[17] Cattaneo, C., Sulla conduzionedelcalore, in: *Atti del Seminario Matematico e Fisico dell Universita di Modena e Reggio Emilia*, vol. 3, 1948, pp. 83–101 (1948).

[18] Christov, C.I., On frame indifferent formulation of the Maxwell–Cattaneo model of finite-speed heat conduction, *Mech. Res. Commun.*, 36, 481-486 (2009).

[19] Straughan, B., Thermal convection with the Cattaneo–Christov model, *Int. J. Heat Mass Transf.* 53, 95–98 (2010).

[20] S. Han, L. Zheng, C. Li, X. Zhang, Coupled flow and heat transfer in viscoelastic fluid with Cattaneo–Christov heat flux model, *Appl. Math. Lett.*, 38, 87–93 (2014).

[21] Elsayed, A.F. and O. Anwar Bég, New computational approaches for biophysical heat transfer in tissue under ultrasonic waves: Variational iteration and Chebyschev spectral simulations, *J. Mechanics Medicine Biology,* 14, 3, 1450043.1-1450043.17 (17 pages) (2014).

[22] Mustafa, M., Cattaneo–Christov heatflux model for rotating flow and heat transfer of upper-convected Maxwell fluid, *AIP Adv*. 5, 047109 (2015).

[23] Hayat, T., M. Mustafa,S. A. Shehzad,S. Obaidat, Melting heat transfer in the stagnation-point flow of an upper-convected Maxwell (UCM) fluid past a stretching sheet, *Int J Num Methods Fluids*, 68, 233–243 (2012).

[24] Frizen, V.E. and F. N. Sarapulov, Formation of MHD processes in induction crucible furnace at single-phase supply of inductor, *Russian Electrical Engineering*, 81, 159-164 (2010).

[25] Bhargava, R., S. Sharma, O. Anwar Bég and Zueco, J, Finite element study of nonlinear two-dimensional deoxygenated biomagnetic micropolar flow, *Communications in Nonlinear Science and Numerical Simulation Journal*, 15, 1210-1233 (2010).

[26] Bég, O.A., M. Ferdows, Shamima Islam and M. Nazrul Islam, Numerical simulation of Marangoni magnetohydrodynamic bio-nanofluid convection from a non-isothermal surface with magnetic induction effects: a bio-nanomaterial manufacturing transport model, *J. Mechanics Medicine Biology,* 14, 3, 1450039.1-1450039.32 (32 pages) (2014).

[27] Hoque, M.M., Md Mahmud Alam; M Ferdows, O. Anwar Bég, Numerical simulation of Dean number and curvature effects on magneto-biofluid flow through a curved conduit, *Proc. IMECHE-Part H; J. Engineering in Medicine*, 227 (11):1155-70 (2013).

[28] Bég, O.A., J. Zueco, M. Norouzi, M. Davoodi, A. A. Joneidi, Assma F. Elsayed, Network and Nakamura tridiagonal computational simulation of electrically-conducting biopolymer micro-morphic transport phenomena, *Computers in Biology and Medicine,* 44, 44–56 (2014).

[29] Kim, S.J., I.C. Bang, J. Buongiorno, And L.W. Hu, Study of pool boiling and critical heat flux enhancement in Nanofluids, *Bulletin Of The Polish Academy Of Sciences Technical Sciences,* 55, 20-30 (2007).

[30] Buongiorno, J. and L.W. Hu, Nanofluids for enhanced economics and safety of nuclear reactors, *Massachusetts Institute of Technology, USA Technical Report* (2007).

[31] M. Ciarletta, B. Straughan, Uniqueness and structural stability for the Cattaneo–Christov equations, *Mech. Res. Commun*. 37, 445–447 (2010).

[32] Bég, O.A., S.S. Motsa, M.N. Islam and M. Lockwood, Pseudo-spectral and variational iteration simulation of exothermically-reacting Rivlin-Ericksen viscoelastic flow and heat transfer in a rocket propulsion duct, *Computational Thermal Sciences*, 6, 1, 1-12 (2014).

[33] Buongiorno, J. Convective transport in nanofluids. *ASME J. Heat Transfer* 128, 240–250 (2006).

[34] Hayat, T., Farooq, M. A.Alsaedi and F. Al-Solamy, Impact of Cattaneo-Christov heat flux in the flow over a stretching sheet with variable thickness, *AIP Advances*, 5, 087159 (2015).

[35] Prasad, V.R., S. A. Gaffar and O. Anwar Bég, Non-similar computational solutions for free convection boundary-layer flow of a nanofluid from an isothermal sphere in a non-Darcy porous medium, *J. Nanofluids,* 4, 1–11 (2015).

[36] Salahuddin, T., Malik, M. Y., Hussain, A., Bilal, S., & Awais, M. MHD flow of Cattanneo–Christov heat flux model for Williamson fluid over a stretching sheet with variable thickness: Using numerical approach, *J. Magnetism and Magnetic Materials*, 401, 991-997. (2016).

[37] Akbar, N. S., Abdelhalim Ebaid, and Z. H. Khan, Numerical analysis of magnetic field effects on Eyring-Powell fluid flow towards a stretching sheet, *J. Magnetism and Magnetic Materials* 382 (2015): 355-358 (2015).

[38] Khan, Z. H., Khan, W. A. and Culham, R. J. Estimation of boundary-layer flow of a nanofluid past a stretching sheet: A revised model, *J. Hydrodynamics* (2014). In press

[39] Khan W.A. and I. Pop, Boundary-layer flow of a nanofluid past a stretching sheet, *International Journal of Heat and Mass Transfer*, 53, 2477-2483 (2010).

[40] Wang, C.Y., Free convection on a vertical stretching surface, *ZAMM-Journal of Applied Mathematics and Mechanics*, 69, 418-420 (1989).

[41] Kandasamy, R. P. Loganathan, and P. Puvi Arasu, Scaling group transformation for MHD boundary-layer flow of a nanofluid past a vertical stretching surface in the presence of suction/injection, *Nuclear Engineering and Design*, 241, 2053-2059 (2011).

[42] Gebhart, B. *et al*, Buoyancy-induced Flows and Transport, Hemisphere, Washington, USA (1988).

[43] Gorla, R.S.R., A. J. Chamkha and A. Aloraier, Melting heat transfer in a nanofluid flow past a permeable continuous moving surface, *J. Naval Architecture and Marine Engineering*, 2, 83-92 (2011).

[44] Nadeem, S., Rehman, A. *et al*, Asymmetric stagnation flow of a micropolar nanofluid in a moving cylinder, *Math. Prob. Engineering*, Volume 2012, Article ID 378259, 18 pages (2012).

[45] Ibrahim, W. and Shankar, B. MHD boundary layer flow and heat transfer of a nanofluid past a permeable stretching sheet with velocity, thermal and solutal slip boundary conditions. *Computers & Fluids*, 75, 1–10(2013).

[46] Uddin, M.J., O. Anwar Bég, A. Aziz and A. I. M. Ismail, Group analysis of free convection flow of a magnetic nanofluid with chemical reaction, *Math. Prob. Engineering*, 2015, Article ID 621503, 11 pp (2015). doi:10.1155/2015/621503.

[47] Sutton, G.W. and Sherman, G., *Engineering Magnetohydrodynamics*, MacGraw-Hill, New York 91965).

[48] Mustafa, M., Hayat, T., Pop, I., Asghar, S. and Obaidat, S., Stagnation-point flow of a nanofluid towards a stretching sheet, *International Journal Heat and Mass Transfer*, 54, 5588–5594 (2011).